JOURNAL OF GUIDANCE, CONTROL, AND DYNAMICS
Vol. 16, No. 1, January-February 1993

Three-Dimensional Modeling and Control of a Twin-Lift Helicopter System

Manoj Mittal and J. V. R. Prasad
Georgia Institute of Technology, Atlanta, Georgia 30332

A twin-lift system offers an efficient and economically attractive solution to the heavy lift problem. A three-dimensional model including the rigid-body dynamics of the two helicopters, the spreader bar, and the load is developed. The mathematical model for helicopter aerodynamics consists of generic, nonlinear, force, and moment models for each helicopter component: main rotor, tail rotor, fuselage, and empennage. The spreader bar and load aerodynamics are also included in the system model. Using the comprehensive system model, a nonlinear controller based on approximate input-output feedback linearization is synthesized. The nonlinear feedback law forms an outer loop for the twin-lift flight control system and is used in conjunction with the existing stability augmentation systems of the helicopters, which constitute the inner loop for the flight control system. The controller performance is illustrated by a closed-loop simulation of a typical twin-lift mission.

Introduction

THE chief motivation for using multilift can be attributed to the promise of obtaining increased productivity without having to manufacture larger and more expensive helicopters.[1] A specific case of multilift arrangement wherein two helicopters jointly transport payloads has been named "twin-lift" and it has been in existence in the helicopter industry for more than two decades. A sketch of a twin-lift helicopter configuration is given in Fig. 1. In the few instances in which the twin-lift concept has been operationally tried, the pilot opinion of maneuvering the system in a completely manual mode has not been favorable, primarily due to the significant increase in cockpit work load. The need for an automatic flight control system for twin-lift operations has thus been suggested. Furthermore, based on a two-dimensional study, Ref. 1 illustrates the fact that a controller should take into account the nonlinearity present in the dynamics; a linear controller synthesized using a linearized model of the twin-lift system yields unsatisfactory performance for operating conditions away from the equilibrium point. In the present work, the rudimentary concept of the nonlinear control technique proposed in Ref. 1 is advanced further. The theoretical development of a nonlinear control law based on a fully nonlinear three-dimensional twin-lift model is given.

Nonlinear Dynamical Model

A comprehensive dynamical model of the twin-lift system is needed for simulation capability as well as for nonlinear control based feedback design. The model should include the rigid-body nonlinear dynamical terms in their entirety for adequate evaluation of controller design. For the twin-lift configuration shown in Fig. 1, the fuselage of each helicopter, the spreader bar, and the load each have six degrees of freedom for rigid-body motion in three-dimensional space. This configuration can be modeled as four rigid bodies interconnected by straight-line links or cables that can be assumed to be elastic or inelastic. The general nonlinear dynamical model derived in this section is valid for elastic cables, with the inelastic cable(s) case being a specialization of this model.

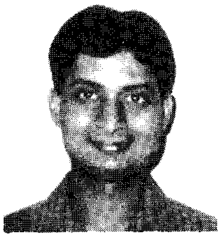

Manoj Mittal received a B.Tech. degree in Aeronautical Engineering from the Indian Institute of Technology at Kanpur in 1986, and M.S. and Ph.D. degrees in Aerospace Engineering from the Georgia Institute of Technology in 1989 and 1991, respectively. He is currently working as a Post-Doctoral Fellow in the School of Aerospace Engineering at Georgia Tech. His research interests include flight dynamics, stability and control, rotorcraft parameter identification, nonlinear control, and adaptive control.

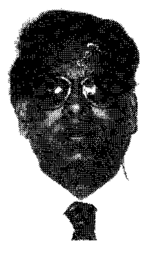

J. V. R. Prasad received his B.Tech and M.S. degrees in Aeronautical Engineering from the Indian Institute of Technology, Madras, India, in 1974 and 1982, respectively, and the Ph.D. degree in Aerospace Engineering from the Georgia Institute of Technology, Atlanta, Georgia, in 1985. He was with the Helicopter Design Bureau of Hindustan Aeronautics Limited, Bangalore, India, as an Aeronautical Engineer from 1975 to 1980 and as a Deputy Design Engineer from 1980 to 1982. He worked as a Research Associate in the School of Aerospace Engineering at Georgia Tech from 1985 to 1987. Since then, he has been an Assistant Professor in the Flight Mechanics and Control area in the School of Aerospace Engineering at Georgia Tech. His research interests include flight vehicle modeling and simulation, atmospheric turbulence modeling and simulation, and applications of linear and nonlinear control theories. He is a Senior Member of AIAA and a Member of AHS.

Received July 23, 1991; presented as Paper 91-2754 at the AIAA Guidance, Navigation, and Control Conference, New Orleans, LA, Aug. 12-14, 1991; revision received April 3, 1992; accepted for publication April 7, 1992.

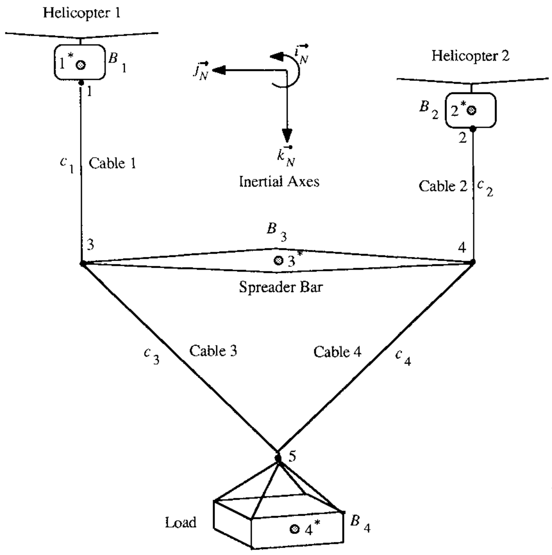

Fig. 1 Twin-lift helicopter configuration.

Some detailed ideas for nonlinear modeling of rigid-body dynamics of the helicopter fuselage, the load, the cable, and the spreader bar are presented by Cicolani and Kanning.[2] In Ref. 2 the equations of motion for a general configuration of the twin-lift system are derived using D'Alembert's principle in conjunction with the virtual work principle and generalized coordinates. Based on a Newton-Euler scheme, a new formulation for the equations of motion is derived in this section. The equations of motion in the two models are written using different sets of coordinates. In the formulation of Ref. 2 the generalized velocity coordinates consist of the center of gravity (c.g.) inertial velocity components of one reference body, the cable velocity components, and the angular velocity components of each body. Similarly, the generalized position coordinates consist of the c.g. inertial position components of one reference body, the orientation angles of the cables, and the orientation angles of each body. In the present formulation the equations of motion are written in terms of the inertial position and velocity components of each body, and the Euler angles and angular velocity components are written in terms of each rigid body. It will be noted in the section on nonlinear control design that, from the point of view of developing a nonlinear controller for the twin-lift system, the coordinates of interest are a linear combination of a subset of the body inertial position coordinates and Euler angles.

The nomenclature adopted for referencing the components of the twin-lift configuration is similar to that employed in Ref. 2 and is described in Fig. 1. The following assumptions are made in the development of the equations of motion:

1) The Earth is flat and nonrotating. The Newtonian/inertial reference frame F_N is fixed to the Earth.

2) The inertial and aerodynamic effects of the cables are neglected. Also, the cables are rigid in transverse motion; i.e., only the longitudinal elasticity is considered. These assumptions on the cable characteristics are validated in Ref. 3.

3) The cables never collapse or slacken.

4) Attachment points 1-5 are frictionless ball and socket joints.

Let $\vec{i}_N$, $\vec{j}_N$, $\vec{k}_N$ be the unit vectors along a set of Cartesian coordinate axes, x', y', z', fixed in F_N. For $n = 1, \ldots, 4$, let F_n denote a reference frame attached to body B_n. The n^* denotes the c.g. of body B_n. Let $\vec{i}_n$, $\vec{j}_n$, $\vec{k}_n$ be unit vectors along a set of Cartesian coordinate axes x_n', y_n', z_n' located at n^* and fixed in F_n. The axes x_n', y_n', z_n' are the body axes of body B_n. Let m_n and $\vec{I}^{(n)}$ denote the mass and central inertia dyadic, respectively, of body B_n. For $n = 1,2$, let F_{c_n} denote a reference frame attached to cable c_n and let $\vec{i}_{c_n}$, $\vec{j}_{c_n}$, $\vec{k}_{c_n}$ be unit vectors along a set of Cartesian coordinate axes x_{c_n}', y_{c_n}', z_{c_n}' fixed in F_{c_n}. For $n = 1, \ldots, 4$, let T_n represent the tension force in cable c_n and let l_n be its instantaneous length. Finally, let $\vec{r}_{ab}$ and $\vec{n}_{ab}$ denote position and unit vectors, respectively, directed from point a to point b.

Equations of Motion

With the assumptions mentioned in the preceding paragraph, the twin-lift system has 24 degrees of freedom. The equations of motion are obtained by first considering vectorial force and moment balance equations of each rigid body. Then the vectorial equations are resolved along appropriate coordinate axes. For body B_i, let x_i, y_i, z_i denote its inertial position coordinates; let $\vec{\omega}^{(i)}$ and $\vec{\alpha}^{(i)}$ denote its angular velocity and angular acceleration, respectively; let $F_x^{(i)}$, $F_y^{(i)}$, $F_z^{(i)}$ denote the inertial axis components of the aerodynamic force acting on it; and let L_i, M_i, N_i denote the body axis components of the aerodynamic moment acting at its c.g. The balance of forces acting on helicopter 1 can be represented by the following equation:

$$(F_x^{(1)} - m_1\ddot{x}_1)\vec{i}_N + (F_y^{(1)} - m_1\ddot{y}_1)\vec{j}_N + (F_z^{(1)} + m_1 g - m_1\ddot{z}_1)\vec{k}_N + T_1\vec{k}_{c_1} = 0 \tag{1}$$

where g is the acceleration due to gravity and an overdot represents a variable's derivative with respect to time. A moment balance of helicopter 1 about the attachment point 1 results in the following equation:

$$\vec{r}_{11^*} \times \left[(F_x^{(1)} - m_1\ddot{x}_1)\vec{i}_N + (F_y^{(1)} - m_1\ddot{y}_1)\vec{j}_N + (F_z^{(1)} + m_1 g - m_1\ddot{z}_1)\vec{k}_N\right] + L_1\vec{i}_1 + M_1\vec{j}_1 + N_1\vec{k}_1 - \vec{\alpha}^{(1)}\cdot\vec{I}^{(1)} - \vec{\omega}^{(1)}\times\vec{I}^{(1)}\cdot\vec{\omega}^{(1)} = 0 \tag{2}$$

The force and moment balance equations of helicopter 2 are analogous to those of helicopter 1 and are given by

$$(F_x^{(2)} - m_2\ddot{x}_2)\vec{i}_N + (F_y^{(2)} - m_2\ddot{y}_2)\vec{j}_N + (F_z^{(2)} + m_2 g - m_2\ddot{z}_2)\vec{k}_N + T_2\vec{k}_{c_2} = 0 \tag{3}$$

$$\vec{r}_{22^*} \times \left[(F_x^{(2)} - m_2\ddot{x}_2)\vec{i}_N + (F_y^{(2)} - m_2\ddot{y}_2)\vec{j}_N + (F_z^{(2)} + m_2 g - m_2\ddot{z}_2)\vec{k}_N\right] + L_2\vec{i}_2 + M_2\vec{j}_2 + N_2\vec{k}_2 - \vec{\alpha}^{(2)}\cdot\vec{I}^{(2)} - \vec{\omega}^{(2)}\times\vec{I}^{(2)}\cdot\vec{\omega}^{(2)} = 0 \tag{4}$$

Next, a consideration of the balance of forces acting on the load results in the following equation:

$$(F_x^{(4)} - m_4\ddot{x}_4)\vec{i}_N + (F_y^{(4)} - m_4\ddot{y}_4)\vec{j}_N + (F_z^{(4)} + m_4 g - m_4\ddot{z}_4)\vec{k}_N - T_3\vec{n}_{35} - T_4\vec{n}_{45} = 0 \tag{5}$$

A moment balance of the load about attachment point 5 leads to the following equation:

$$\vec{r}_{54^*} \times \left[(F_x^{(4)} - m_4\ddot{x}_4)\vec{i}_N + (F_y^{(4)} - m_4\ddot{y}_4)\vec{j}_N + (F_z^{(4)} + m_4 g - m_4\ddot{z}_4)\vec{k}_N\right] + L_4\vec{i}_4 + M_4\vec{j}_4 + N_4\vec{k}_4 - \vec{\alpha}^{(4)}\cdot\vec{I}^{(4)} - \vec{\omega}^{(4)}\times\vec{I}^{(4)}\cdot\vec{\omega}^{(4)} = 0 \tag{6}$$

The balance of forces acting on the spreader bar can be represented by the following equation:

$$(F_x^{(3)} - m_3\ddot{x}_3)\vec{i}_N + (F_y^{(3)} - m_3\ddot{y}_3)\vec{j}_N + (F_z^{(3)} + m_3 g - m_3\ddot{z}_3)\vec{k}_N + T_3\vec{n}_{35} - T_4\vec{n}_{45}T_1\vec{k}_{c_1} - T_2\vec{k}_{c_2} = 0 \tag{7}$$

Finally, a moment balance of the spreader bar about attachment point 5 gives rise to the following equation:

$$\vec{r}_{53^*} \times \Big[(F_x^{(3)} - m_3\ddot{x}_3)\vec{i}_N + (F_y^{(3)} - m_3\ddot{y}_3)\vec{j}_N + (F_z^{(3)} + m_3 g - m_3\ddot{z}_3)\vec{k}_N\Big] + \vec{r}_{53} \times (-T_1\vec{k}_{c_1}) + \vec{r}_{54} \times (-T_2\vec{k}_{c_2}) + L_3\vec{i}_3 + M_3\vec{j}_3 + N_3\vec{k}_3 - \vec{\alpha}^{(3)} \cdot \vec{I}^{(3)} - \vec{\omega}^{(3)} \times \vec{I}^{(3)} \cdot \vec{\omega}^{(3)} = 0 \tag{8}$$

The next step in the formulation consists of expressing Eqs. (1-8) in scalar form. To conserve space, the steps involved in this procedure are not shown in the paper, but the interested reader may refer to Ref. 3. Only the final form of the equations is presented here. For $n = 1, \ldots, 4$, let p_n, q_n, r_n represent the body axis components of the angular velocity of body B_n. The scalar components of Eqs. (1) and (3) can be combined to yield the following equations for the ith $(i = 1,2)$ helicopter:

$$(F_x^{(i)} - m_i\ddot{x}_i)z_{iB} - (F_z^{(i)} + m_i g - m_i\ddot{z}_i)x_{iB} = 0 \tag{9}$$

$$(F_x^{(i)} - m_i\ddot{x}_i)y_{iB} - (F_y^{(i)} - m_i\ddot{y}_i)x_{iB} = 0 \tag{10}$$

$$T_i = (F_x^{(i)} - m_i\ddot{x}_i)\frac{x_{iB}}{l_i} + (F_y^{(i)} - m_i\ddot{y}_i)\frac{y_{iB}}{l_i} + (F_z^{(i)} + m_i g - m_i\ddot{z}_i)\frac{z_{iB}}{l_i} \tag{11}$$

and

$$l_i^2 = x_{iB}^2 + y_{iB}^2 + z_{iB}^2 \tag{12}$$

where x_{1B}, y_{1B}, z_{1B} are the inertial axis components of the vector directed from point 1 to point 3 and x_{2B}, y_{2B}, z_{2B} are the inertial axis components of the vector directed from point 2 to point 4. Let $(\psi_i, \theta_i, \phi_i)$ be the Euler angle triplet used to define the orientation of the body axes attached to the ith $(i = 1,2)$ helicopter. Then, combining the scalar components of Eqs. (2) and (4), one gets the following equations for the ith helicopter:

$$\begin{aligned}&\dot{p}_i I_{x_ix_i}^{(i)} + \dot{r}_i I_{x_iz_i}^{(i)} - q_i r_i(I_{y_iy_i}^{(i)} - I_{z_iz_i}^{(i)}) + p_i q_i I_{x_iz_i}^{(i)} \\ &\quad + h_i\Big[(F_x^{(i)} - m_i\ddot{x}_i)(\sin\psi_i\cos\phi_i - \cos\psi_i\sin\theta_i\sin\phi_i) \\ &\quad - (F_y^{(i)} - m_i\ddot{y}_i)(\sin\psi_i\sin\theta_i\sin\phi_i + \cos\psi_i\cos\phi_i) \\ &\quad - (F_z^{(i)} + m_i g - m_i\ddot{z}_i)\cos\theta_i\sin\phi_i\Big] - L_i = 0\end{aligned} \tag{13}$$

$$\begin{aligned}&\dot{q}_i I_{y_iy_i}^{(i)} - p_i r_i(I_{z_iz_i}^{(i)} - I_{x_ix_i}^{(i)}) + (r_i^2 - p_i^2)I_{x_iz_i}^{(i)} \\ &\quad + h_i\Big[(F_x^{(i)} - m_i\ddot{x}_i)\cos\psi_i\cos\theta_i + (F_y^{(i)} - m_i\ddot{y}_i)\sin\psi_i\cos\theta_i \\ &\quad - (F_z^{(i)} + m_i g - m_i\ddot{z}_i)\sin\theta_i\Big] - M_i = 0\end{aligned} \tag{14}$$

$$\dot{r}_i I_{z_iz_i}^{(i)} + \dot{p}_i I_{x_iz_i}^{(i)} - p_i q_i(I_{x_ix_i}^{(i)} - I_{y_iy_i}^{(i)}) - q_i r_i I_{x_iz_i}^{(i)} - N_i = 0 \tag{15}$$

In Eqs. (13) and (14) h_i is defined by the relation $\vec{r}^{\,i^*i} = h_i\vec{k}_i$. Consider the geometry of the triangle made by the spreader bar axis and the bridle cables c_3 and c_4. Suppose the plane of this triangle at any time instant is as shown in Fig. 2. Let $(\psi_3, \phi_3, \theta_3)$ and $(\psi_t, \phi_t, \theta_t)$ denote the Euler angle triplets used to define the orientation of the Cartesian coordinate axes attached to the spreader bar and to the triangle, respectively. Let δ_1 be the in-plane angle between the spreader bar axis and cable c_3, and let δ_2 be the in-plane angle between the spreader bar axis and cable c_4. Then the scalar components of the load force balance equation [Eq. (5)] are given as

$$\begin{aligned}&(F_x^{(4)} - m_4\ddot{x}_4)(\cos\psi_3\cos\theta_t - \sin\psi_3\sin\phi_3\sin\theta_t) \\ &\quad + (F_y^{(4)} - m_4\ddot{y}_4)(\sin\psi_3\cos\theta_t + \cos\psi_3\sin\phi_3\sin\theta_t) \\ &\quad - (F_z^{(4)} + m_4 g - m_4\ddot{z}_4)\cos\phi_3\sin\theta_t = 0\end{aligned} \tag{16}$$

$$\begin{aligned}&(F_x^{(4)} - m_4\ddot{x}_4)\sin\psi_3\cos\phi_3 - (F_y^{(4)} - m_4\ddot{y}_4)\cos\psi_3\cos\phi_3 \\ &\quad - (F_z^{(4)} + m_4 g - m_4\ddot{z}_4)\sin\phi_3 = T_3\cos\delta_1 - T_4\cos\delta_2\end{aligned} \tag{17}$$

$$\begin{aligned}&(F_x^{(4)} - m_4\ddot{x}_4)(\cos\psi_3\sin\theta_t + \sin\psi_3\sin\phi_3\cos\theta_t) \\ &\quad + (F_y^{(4)} - m_4\ddot{y}_4)(\sin\psi_3\sin\theta_t - \cos\psi_3\sin\phi_3\cos\theta_t) \\ &\quad + (F_z^{(4)} + m_4 g - m_4\ddot{z}_4)\cos\phi_3\cos\theta_t = T_3\sin\delta_1 + T_4\sin\delta_2\end{aligned} \tag{18}$$

Let l_y and l_z represent the y and z components of the position vector directed from 3* to 5 when it is resolved in the coordinate axes attached to the triangle frame. The length of cables c_3 and c_4 can be expressed as

$$l_3^2 = \left(\frac{L}{2} - l_y\right)^2 + l_z^2, \qquad l_4^2 = \left(\frac{L}{2} + l_y\right)^2 + l_z^2 \tag{19}$$

In Eqs. (19), L is defined by the relation $\vec{r}^{\,43} = L\vec{j}_3$. Let $(\psi_4, \theta_4, \phi_4)$ denote the Euler angle triplet used to define the orientation of the coordinate axes attached to the load. Assuming that the load body axes are also the central principal axes for the load, the scalar components of Eq. (6) are

$$\begin{aligned}&\dot{p}_4 I_{x_4x_4}^{(4)} - q_4 r_4(I_{y_4y_4}^{(4)} - I_{z_4z_4}^{(4)}) \\ &\quad - l\Big[(F_x^{(4)} - m_4\ddot{x}_4)(\sin\psi_4\cos\phi_4 - \cos\psi_4\sin\theta_4\sin\phi_4) \\ &\quad - (F_y^{(4)} - m_4\ddot{y}_4)(\sin\psi_4\sin\theta_4\sin\phi_4 + \cos\psi_4\cos\phi_4) \\ &\quad - (F_z^{(4)} + m_4 g - m_4\ddot{z}_4)\cos\theta_4\sin\phi_4\Big] - L_4 = 0\end{aligned} \tag{20}$$

$$\begin{aligned}&\dot{q}_4 I_{y_4y_4}^{(4)} - p_4 r_4(I_{z_4z_4}^{(4)} - I_{x_4x_4}^{(4)}) - l\Big[(F_x^{(4)} - m_4\ddot{x}_4)\cos\psi_4\cos\theta_4 \\ &\quad + (F_y^{(4)} - m_4\ddot{y}_4)\sin\psi_4\cos\theta_4 - (F_z^{(4)} + m_4 g \\ &\quad - m_4\ddot{z}_4)\sin\theta_4\Big] - M_4 = 0\end{aligned} \tag{21}$$

$$\dot{r}_4 I_{z_4z_4}^{(4)} - p_4 q_4(I_{x_4x_4}^{(4)} - I_{y_4y_4}^{(4)}) - N_4 = 0 \tag{22}$$

In Eqs. (20) and (21), l is defined by the relation $\vec{r}^{\,5^*4} = l\vec{k}_4$. The scalar components of the spreader bar force balance equation [Eq. (7)] are given as

$$m_1\ddot{x}_1 + m_2\ddot{x}_2 + m_3\ddot{x}_3 + m_4\ddot{x}_4 = F_x^{(1)} + F_x^{(2)} + F_x^{(3)} + F_x^{(4)} \tag{23}$$

$$m_1\ddot{y}_1 + m_2\ddot{y}_2 + m_3\ddot{y}_3 + m_4\ddot{y}_4 = F_y^{(1)} + F_y^{(2)} + F_y^{(3)} + F_y^{(4)} \tag{24}$$

$$m_1\ddot{z}_1 + m_2\ddot{z}_2 + m_3\ddot{z}_3 + m_4\ddot{z}_4 = F_z^{(1)} + F_z^{(2)} + F_z^{(3)} + F_z^{(4)} + (m_1 + m_2 + m_3 + m_4)g \tag{25}$$

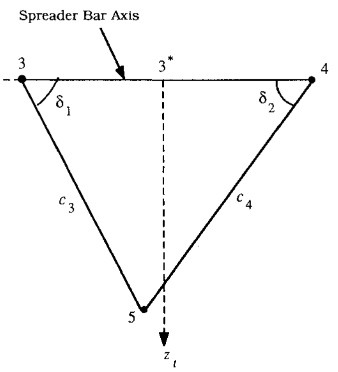

Fig. 2 Triangle made by spreader bar axis and cables c_3 and c_4.

Assuming that the spreader bar body axes are also the central principal axes for the spreader bar, the scalar components of Eq. (8) are

$$\dot{p}_3 I^{(3)}_{x_3x_3} - q_3 r_3 (I^{(3)}_{y_3y_3} - I^{(3)}_{z_3z_3}) - (\cos\psi_3 \sin\theta_3 + \sin\psi_3 \cos\theta_3 \sin\phi_3)\left[\frac{L}{2}\{F^{(1)}_x - m_1\ddot{x}_1 - (F^{(2)}_x - m_2\ddot{x}_2)\} + l_y(F^{(4)}_x - m_4\ddot{x}_4)\right]$$
$$- (\sin\psi_3 \sin\theta_3 - \cos\psi_3 \cos\theta_3 \sin\phi_3)\left[\frac{L}{2}\{F^{(1)}_y - m_1\ddot{y}_1 - (F^{(2)}_y - m_2\ddot{y}_2)\} + l_y(F^{(4)}_y - m_4\ddot{y}_4)\right]$$
$$- \cos\theta_3 \cos\phi_3\left[\frac{L}{2}\{F^{(1)}_z + m_1 g - m_1\ddot{z}_1 - (F^{(2)}_z + m_2 g - m_2\ddot{z}_2)\} + l_y(F^{(4)}_z + m_4 g - m_4\ddot{z}_4)\right]$$
$$- l_z\left[(F^{(4)}_x - m_4\ddot{x}_4)\sin\psi_3\cos\phi_3 - (F^{(4)}_y - m_4\ddot{y}_4)\cos\psi_3\cos\phi_3 - (F^{(4)}_z + m_4 g - m_4\ddot{z}_4)\sin\phi_3\right]\cos(\theta_t - \theta_3) - L_3 = 0 \tag{26}$$

$$\dot{q}_3 I^{(3)}_{y_3y_3} - p_3 r_3 (I^{(3)}_{z_3z_3} - I^{(3)}_{x_3x_3}) - l_z\left[(F^{(4)}_x - m_4\ddot{x}_4)(\cos\psi_3\cos\theta_t - \sin\psi_3\sin\phi_3\sin\theta_t)\right.$$
$$\left. + (F^{(4)}_y - m_4\ddot{y}_4)(\sin\psi_3\cos\theta_t + \cos\psi_3\sin\phi_3\sin\theta_t) - (F^{(4)}_z + m_4 g - m_4\ddot{z}_4)\cos\phi_3\sin\theta_t\right] - M_3 = 0 \tag{27}$$

$$\dot{r}_3 I^{(3)}_{z_3z_3} - p_3 q_3 (I^{(3)}_{x_3x_3} - I^{(3)}_{y_3y_3}) + (\cos\psi_3 \cos\theta_3 - \sin\psi_3 \sin\theta_3 \sin\phi_3)\left[\frac{L}{2}\{F^{(1)}_x - m_1\ddot{x}_1 - (F^{(2)}_x - m_2\ddot{x}_2)\} + l_y(F^{(4)}_x - m_4\ddot{x}_4)\right]$$
$$+ (\sin\psi_3 \cos\theta_3 + \cos\psi_3 \sin\phi_3 \sin\theta_3)\left[\frac{L}{2}\{F^{(1)}_y - m_1\ddot{y}_1 - (F^{(2)}_y - m_2\ddot{y}_2)\} + l_y(F^{(4)}_y - m_4\ddot{y}_4)\right]$$
$$- \cos\phi_3 \sin\theta_3\left[\frac{L}{2}\{F^{(1)}_z + m_1 g - m_1\ddot{z}_1 - (F^{(2)}_z + m_2 g - m_2\ddot{z}_2)\} + l_y(F^{(4)}_z + m_4 g - m_4\ddot{z}_4)\right]$$
$$+ l_z\left[(F^{(4)}_x - m_4\ddot{x}_4)\sin\psi_3\cos\phi_3 - (F^{(4)}_y - m_4\ddot{y}_4)\cos\psi_3\cos\phi_3 - (F^{(4)}_z + m_4 g - m_4\ddot{z}_4)\sin\phi_3\right]\sin(\theta_t - \theta_3) - N_3 = 0 \tag{28}$$

Elastic vs Inelastic Cables

Equations (9–11), (13–18), and (20–28) furnish a set of nonlinear equations of motion for the twin-lift system. The distinction between the case involving elastic cables and that involving inelastic cables can be made very easily at this point. For the case of elastic cables, the cable tension forces T_i, $i = 1,\ldots,4$ present in Eqs. (11), (17), and (18) are substituted for in terms of the following constitutive laws:

$$T_i = \max\left[0,\ k_i(l_i - l_{i_0})\right], \qquad i = 1,\ldots,4 \tag{29}$$

where k_i is the stiffness constant for cable c_i and l_{i_0} is its unloaded length. On the other hand, for inelastic cables, the aforementioned four equations can simply be dropped from the formulation. However, these equations can be used to calculate the cable tension forces as dependent quantities. It is noted that for a case involving inelastic cables, the number of degrees of freedom in the system is reduced by four and for this case there are four kinematic constraint relationships, given by Eqs. (12) and (19). However, it is very difficult and tedious to use the four constraint equations to solve explicitly for four variables. Instead, it is preferable to simply differentiate these equations twice with respect to time and incorporate them as second-order ordinary differential equations along with the remaining set. This represents treating a set of holonomic constraints as a set of pseudo-nonholonomic constraints.[4]

Kinematic Equations

To complete the formulation of the dynamics of the helicopter fuselage, load, spreader bar, and the cables constituting the twin-lift system, the kinematic differential relationship between the following pair of variables representing angular motion and rate, respectively, is required: $(\psi_n, \theta_n, \phi_n)$ and (p_n, q_n, r_n), $n = 1,\ldots,4$. For bodies B_1, B_2, and B_4, the required relationship is obtained by considering a sequence of z-y-x body-fixed rotations. The resulting equations are

$$\begin{Bmatrix} p_n \\ q_n \\ r_n \end{Bmatrix} = \begin{bmatrix} 1 & 0 & -\sin\theta_n \\ 0 & \cos\phi_n & \cos\theta_n\sin\phi_n \\ 0 & -\sin\phi_n & \cos\theta_n\cos\phi_n \end{bmatrix} \begin{Bmatrix} \dot{\phi}_n \\ \dot{\theta}_n \\ \dot{\psi}_n \end{Bmatrix}$$

$$n = 1,2,4 \tag{30}$$

For body B_3, which is the spreader bar, a z-x-y body-fixed rotation sequence is employed. This rotation sequence makes use of the fact that the bridle cables form a triangle with the spreader bar axis; this implies that the orientation of the bar differs from that of the triangle by at most one rotation, which is about the bar y axis. The equation for the spreader bar kinematics can be written as

$$\begin{Bmatrix} p_3 \\ q_3 \\ r_3 \end{Bmatrix} = \begin{bmatrix} \cos\theta_3 & 0 & -\cos\phi_3\sin\theta_3 \\ 0 & 1 & \sin\phi_3 \\ \sin\theta_3 & 0 & \cos\phi_3\cos\theta_3 \end{bmatrix} \begin{Bmatrix} \dot{\phi}_3 \\ \dot{\theta}_3 \\ \dot{\psi}_3 \end{Bmatrix} \tag{31}$$

Model Validation

The nonlinear model of the twin-lift system described in this section was reduced to a case involving only two-dimensional lateral/vertical motion of the entire system. The resulting equations were further simplified to a case involving inelastic cables and zero load attachment point distance ($l = 0$). The resulting two-dimensional model of the twin-lift system matched perfectly with an earlier one presented in Ref. 5 that was derived independently under the same assumptions and conditions. The model in Ref. 5 was derived using a Newton-Euler scheme. This provided confidence in the validity of the present model. Also, the nonlinear model for the two-dimensional case was linearized about a hovering condition. The resulting linear model was found to be identical to that of Ref. 6.

The following section contains a brief description of the aerodynamic models used for various components of the twin-lift configuration: the helicopters, the spreader bar, and the load.

Aerodynamic Models

Helicopters

The aerodynamic model for helicopters described in Ref. 7 is used in this paper. It consists of generic, nonlinear, force, and moment models for each helicopter component: main rotor, tail rotor, fuselage, and empennage. Since adequate documentation is available for this model, and because it involves extremely lengthy equations, a description of the model is unwarranted. This aerodynamic model is used in the present work with the simplification that the main rotor flapping motion is assumed to be quasisteady. This assumption is typical of simulation models for slung load systems.[2,8]

Load

In Ref. 8, explicit expressions for aerodynamic forces and moments are obtained for the $8 \times 8 \times 20$-ft cargo container by fitting trigonometric functions to wind-tunnel data acquired for a scale model in an earlier study. In the present work the load is assumed to be enclosed in this rectangular-shaped cargo container, and its aerodynamic model is used in the simulation. This type of load is a convenient example for numerical simulation and controller evaluation for the twin-lift system and exemplifies aerodynamic behavior for a large group of loads. For further details about the load aerodynamic model, the reader is referred to Ref. 8.

Spreader Bar

No detailed measurements or calculations of spreader bar aerodynamic loads exist in the literature. However, as a first cut at the analysis, the spreader bar aerodynamics can be modeled in terms of its equivalent flat-plate area.[9] Using this concept, and assuming that the bar is a nonlifting surface, the total force acting at its c.g. is the drag force, which can be expressed as

$$\bar{D}^{(3)} = -(\tfrac{1}{2})\rho\left(u_3^2 S_x^{(3)} c_{D_x}^{(3)} \bar{i}_3 + v_3^2 S_y^{(3)} c_{D_y}^{(3)} \bar{j}_3 + w_3^2 S_z^{(3)} c_{D_z}^{(3)} \bar{k}_3\right) \quad (32)$$

where ρ is the density of air, $c_{D_x}^{(3)}$, $c_{D_y}^{(3)}$, $c_{D_z}^{(3)}$ are the drag coefficients associated with the x, y, z faces of the spreader bar, and $S_x^{(3)}$, $S_y^{(3)}$, $S_z^{(3)}$ are the surface areas of the x, y, z faces of the spreader bar. The products $S_x^{(3)} C_{D_x}^{(3)}$, etc., are the equivalent flat-plate areas and once these areas are estimated, the drag force can be readily computed. Since the surface area of a spreader bar is expected to be small, the aerodynamic loads acting on it will be small and this is the rationale for the approximate analysis. Because of lack of a detailed representation, the components of aerodynamic moment acting at the spreader bar c.g. (L_3, M_3, N_3) are assumed to be zero. Clearly, a more detailed aerodynamic representation for the spreader bar can be easily accommodated within the overall system model.

State-Space Representation

The twin-lift model equations discussed in the two preceding sections can be put in a state-space form as follows. A state variable vector, $\boldsymbol{x}$, is defined as

$$\boldsymbol{x} = \left\{\boldsymbol{x}_1^T, \boldsymbol{x}_2^T\right\}^T \quad (33)$$

where

$$\boldsymbol{x}_1 = \left\{x_1, y_1, z_1, \phi_1, \theta_1, \psi_1, x_2, y_2, z_2, \phi_2, \theta_2, \psi_2, x_3, y_3, z_3, \phi_3, \theta_3, \psi_3, x_4, y_4, z_4, \phi_4, \theta_4, \psi_4\right\}^T \quad (34)$$

and

$$\boldsymbol{x}_2 = \left\{\dot{x}_1, \dot{y}_1, \dot{z}_1, p_1, q_1, r_1, \dot{x}_2, \dot{y}_2, \dot{z}_2, p_2, q_2, r_2, \dot{x}_3, \dot{y}_3, \dot{z}_3, p_3, q_3, r_3, \dot{x}_4, \dot{y}_4, \dot{z}_4, p_4, q_4, r_4\right\}^T \quad (35)$$

A control vector,

$$\boldsymbol{u} = \left\{\theta_0^{(1)}, A_{1s}^{(1)}, B_{1s}^{(1)}, \theta_{0_{TR}}^{(1)}, \theta_0^{(2)}, A_{1s}^{(2)}, B_{1s}^{(2)}, \theta_{0_{TR}}^{(2)}\right\}^T \quad (36)$$

is defined where θ_0 is the main rotor collective pitch, A_{1s} and B_{1s} are the lateral and longitudinal cyclic angles in the hub-body axis system, and $\theta_{0_{TR}}$ is the tail rotor collective pitch. The equations corresponding to the force and moment balance of the helicopters, the spreader bar, and the load can be written in the following form:

$$\dot{\boldsymbol{x}}_1 = \boldsymbol{E}(\boldsymbol{x}_1)\boldsymbol{x}_2 \quad (37)$$

$$\boldsymbol{M}(\boldsymbol{x}_1)\dot{\boldsymbol{x}}_2 = \boldsymbol{r}(\boldsymbol{x}_1, \boldsymbol{x}_2, \boldsymbol{a}) + \boldsymbol{S}(\boldsymbol{x}_1, \boldsymbol{x}_2, \boldsymbol{a})\boldsymbol{u} \quad (38)$$

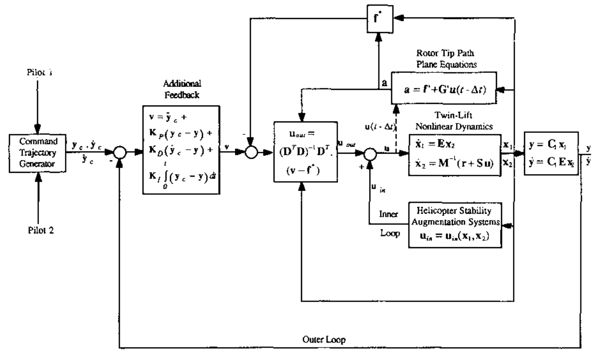

Fig. 3 Twin-lift inner and outer loop control structure.

The equations describing the tip-path plane motion of the main and tail rotors of the two helicopters can be written as

$$\boldsymbol{a} = \boldsymbol{f}'(\boldsymbol{x}_1, \boldsymbol{x}_2) + \boldsymbol{G}'(\boldsymbol{x}_1, \boldsymbol{x}_2)\boldsymbol{u} \quad (39)$$

where

$$\boldsymbol{a} = \left\{a_0^{(1)}, a_1^{(1)}, b_1^{(1)}, a_{1_{TR_C}}^{(1)}, b_{1_{TR_C}}^{(1)}, a_0^{(2)}, a_1^{(2)}, b_1^{(2)}, a_{1_{TR_C}}^{(2)}, b_{1_{TR_C}}^{(2)}\right\} \quad (40)$$

In Eq. (40), a_0, a_1, and b_1 are, respectively, the coning angle, the longitudinal flapping coefficient, and the lateral flapping coefficient of the main rotor measured from its hub plane; and $a_{1_{TR_C}}$ and $b_{1_{TR_C}}$ are the longitudinal and lateral first harmonic flapping coefficients of the tail rotor measured from its hub plane. In Eq. (37), $\boldsymbol{E}$ is a 24×24 matrix; in Eq. (38), $\boldsymbol{M}$ is a 24×24 matrix, $\boldsymbol{r}$ is a 24×1 vector, and $\boldsymbol{S}$ is a 24×8 matrix. In Eq. (39), $\boldsymbol{f}'$ is a 10×1 vector and $\boldsymbol{G}'$ is a 10×8 matrix. Detailed expressions for $\boldsymbol{E}$, $\boldsymbol{M}$, $\boldsymbol{r}$, $\boldsymbol{S}$, $\boldsymbol{f}'$, and $\boldsymbol{G}'$ are given in Ref. 3.

An assumption is made regarding Eq. (39) in the ensuing analysis. It is assumed that the value of $\boldsymbol{a}(t)$ depends on a lagged value of the control, $\boldsymbol{u}(t - \Delta t)$, instead of the instantaneous value of the control, $\boldsymbol{u}(t)$. In other words, Eq. (39) is replaced by the following equation:

$$\boldsymbol{a}(t) = \boldsymbol{f}'(\boldsymbol{x}_1, \boldsymbol{x}_2) + \boldsymbol{G}'(\boldsymbol{x}_1, \boldsymbol{x}_2)\boldsymbol{u}(t - \Delta t) \quad (41)$$

Note that the state vector of the system, $\boldsymbol{x}(t)$, also depends on $\boldsymbol{u}(t - \Delta t)$. It is felt that, compared to Eq. (39), Eq. (41) is a better approximation to the original second-order ordinary differential equation governing the evolution of $\boldsymbol{a}$. The assumption is reasonable if Δt is smaller than the time lag involved in the steady-state response of $\boldsymbol{a}$ due to control input application. In the simplest analysis, Δt can be taken to be equal to the simulation time step, provided the latter is sufficiently small. The assumption is also useful for the development of a nonlinear feedback controller based on the method of input-output feedback linearization, discussed in the following section. The method requires the control inputs to enter the system dynamic equations linearly. However, a careful scrutiny reveals that, if Eq. (39) is substituted into the equation of motion [Eq. (38)], the resulting dynamic equations will no longer be linear (or affine) in the control variable $\boldsymbol{u}$. It is pointed out that this is only due to the quasisteady representation of the rotor flapping dynamics. If the computed value of $\boldsymbol{a}(t)$ as given by Eq. (41) is utilized in Eq. (38), the control design method can still be used to calculate an input-output linearizing control, $u(t)$. It is worth noting that, if the original second-order differential equation were to be used to describe the evolution of $a(t)$, then the components of a [given by Eq. (40)] would have been states of the overall system and the complete set of dynamic equations would indeed have been affine in u. However, using such a model for control design would imply higher computational work load by the controller.

The next section outlines the synthesis of a nonlinear flight control system for the twin-lift configuration.

Nonlinear Control

Similar to what has been envisaged in Ref. 10, the structure of the twin-lift flight control system is as follows. At the very top level, the twin-lift controller interprets the pilots' commands for maneuvering the system. These commands can be in the form of either final conditions desired by the pilot or real-time pilot-generated command trajectories. In the first case the flight control system will produce command trajectories internally. Note that, in either case, the task of generating controller commands can be shared by the pilots in a predetermined fashion. At the second level, the flight control system collects state information from the twin-lift configuration and generates control inputs for the two helicopters. These inputs are then combined with the control inputs produced by the individual helicopters' stability augmentation systems (SASs), and the resulting inputs are fed into the helicopters. The SAS of a helicopter is a component of its automatic flight control system. Thus, the twin-lift controller may be regarded as an outer feedback loop for each helicopter, whereas its SAS constitutes an inner feedback loop. The outer loop feedback design is undertaken in the following. The existing SAS of each helicopter is employed as such, without any alteration.

The total control vector may be regarded as the sum of inner and outer loop components:

$$u = u_{\text{in}} + u_{\text{out}} \tag{42}$$

The inner loop control u_{in} is dependent on the SASs of the individual helicopters. In general, u_{in} can be functionally expressed as

$$u_{\text{in}} = u_{\text{in}}(x_1, x_2) \tag{43}$$

For example, the SAS of a typical channel helicopter consists of vertical velocity feedback for the collective stick input; pitch rate and pitch attitude feedbacks for the longitudinal channel; roll rate and bank angle feedbacks for the lateral channel; and

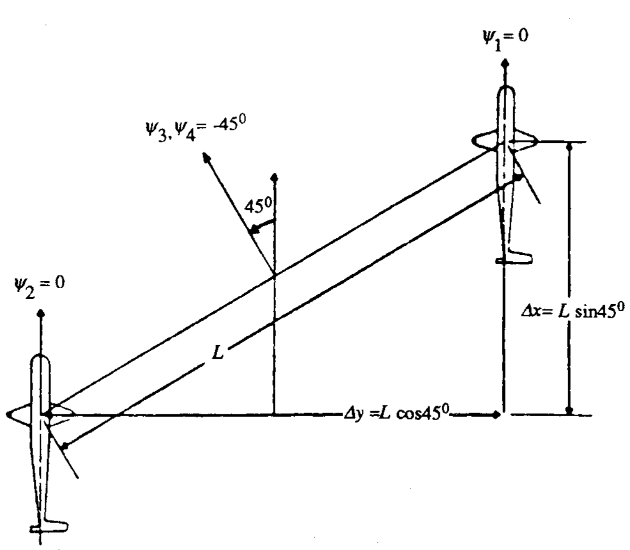

Fig. 4 Typical configuration of twin-lift operation.

Table 1 Numerical values of physical parameters used in the analysis

Parameter	Value
h_1, h_2	3.6 ft
l	20 ft
L	107.32 ft
l_1, l_2	50.0 ft
l_3, l_4	75.89 ft
m_3	30 slugs
$I^{(3)}_{x_3x_3}, I^{(3)}_{z_3z_3}$	28840.83 slugs-ft^2
$I^{(3)}_{y_3y_3}$	93.75 slugs-ft^2
S_{x_3}, S_{z_3}	5.0 ft^2
S_{y_3}	1.0 ft^2
$c_{D_{x_3}}, c_{D_{y_3}}, c_{D_{z_3}}$	1.0
m_4	734.59 slugs
$I^{(4)}_{x_4x_4}$	3151.4 slugs-ft^2
$I^{(4)}_{y_4y_4}, I^{(4)}_{z_4z_4}$	39709.96 slugs-ft^2

yaw rate feedback for the directional channel. All of these feedback loops are closed through constant gain elements. Thus, the inner loop component of the helicopter controls can be expressed as

$$\left.\begin{aligned} \Delta\delta_c^{(i)} &= -K_w^{(i)}\Delta w_i \\ \Delta\delta_e^{(i)} &= -K_q^{(i)}\Delta q_i - K_\theta^{(i)}\Delta\theta_i \\ \Delta\delta_a^{(i)} &= -K_p^{(i)}\Delta p_i - K_\phi^{(i)}\Delta\phi_i \\ \Delta\delta_p^{(i)} &= -K_r^{(i)}\Delta r_i \end{aligned}\right\} \quad i = 1,2 \tag{44}$$

where $\Delta(\ )$ denotes perturbation value of ( ) from a trim condition, and the K represent constant gains. The δ_c, δ_e, δ_a, δ_p are respectively the collective stick input, the longitudinal cyclic stick input, the lateral cyclic stick input, and the pedal input. The cockpit controls are related to the blade pitch angles by the following linear, constant transformation:

$$u = L\delta + b \tag{45}$$

where

$$\delta = \{\delta_c^{(1)}, \delta_e^{(1)}, \delta_a^{(1)}, \delta_p^{(1)}, \delta_c^{(2)}, \delta_e^{(2)}, \delta_a^{(2)}, \delta_p^{(2)}\}^T \tag{46}$$

When Eqs. (42) and (43) are substituted into Eqs. (37) and (38), the result is

$$\begin{Bmatrix} \dot{x}_1 \\ \dot{x}_2 \end{Bmatrix} = \begin{Bmatrix} E(x_1)x_2 \\ M^{-1}(x_1)\left[r(x_1,x_2,a) + S(x_1,x_2,a)u_{\text{in}}(x_1,x_2)\right] \end{Bmatrix} + \begin{bmatrix} 0 \\ M^{-1}(x_1)S(x_1,x_2,a) \end{bmatrix} u_{\text{out}} \tag{47}$$

Equations (47) and (41) together constitute a state-space representation of the twin-lift system.

The control design technique used here is based on seeking linear input-output system behavior through nonlinear state feedback. Several names have been proposed for this technique (e.g., input-output feedback linearization, nonlinear inverse dynamics, nonlinear decoupling, and noninteracting control). The control of nonlinear systems through the use of their inverse dynamics is a topic that has recently received a great deal of attention. In Ref. 11 the necessary and sufficient condition for decoupling a class of square nonlinear systems, in which the outputs are linear functions of the states, is obtained. It is shown that, when this condition is satisfied, a state feedback control law exists that makes each output variable of the dynamic system independently controllable with a separate input. To use the theory given in Ref. 11, one needs first to define the output variables. Naturally, these should be the variables receiving the highest priority to be controlled. The selection of these variables becomes straightforward once the objective of the twin-lift mission is clearly understood.

The primary objective of the twin-lift mission is to transport the load to any desired position in a specified time interval. This can be achieved by first commanding the average longitudinal and lateral positions of the helicopters defined by

$$\bar{x} = \frac{x_1 + x_2}{2}, \qquad \bar{y} = \frac{y_1 + y_2}{2} \tag{48}$$

and the vertical position of the load, z_4. Then, by introducing two more output variables, $x_4 - \bar{x}$ and $y_4 - \bar{y}$, it is ensured that the actual load longitudinal and lateral positions are regulated close to their commanded values. Note that the load longitudinal and lateral positions are not controlled directly because of their weak dependence on the helicopter controls. For example, in a symmetric hovering condition when the cables c_1 and c_2 are nearly vertical, only the vertical position of the load can be controlled directly by the helicopters. This is due to the fact that the cables'support forces only along the lengthwise direction. If either x_4 or y_4 is controlled directly from a symmetric hovering condition with cables c_1 and c_2 vertical, then the helicopter controls saturate for small command values.

It is vital that the maneuvering be carried out while maintaining safe longitudinal, lateral, and vertical separation distances between the helicopters in order to prevent them from colliding. This can be achieved by regulating the helicopter c.g. separation distances defined by

$$\Delta x = x_1 - x_2, \qquad \Delta y = y_1 - y_2, \qquad \Delta z = z_1 - z_2 \tag{49}$$

about a predetermined set of values. Ideally, one would like to construct an output vector consisting of the eight variables discussed earlier and proceed with the application of nonlinear decoupling results obtained in Ref. 11 to the square system thus obtained. However, when the control law obtained using these outputs was implemented in a computer simulation of the twin-lift nonlinear dynamical model, it was found that the closed-loop system became unstable. Hence, a straightforward application of the nonlinear decoupling theory discussed in Ref. 11 did not lead to satisfactory results. It was determined that providing damping to the helicopter attitude dynamics is essential for stable maneuvering of the closed-loop system. Thus, the original output vector was augmented with the Euler angles of each helicopter. The final output vector is

$$y = \{\bar{x}, \bar{y}, z_4, \Delta x, \Delta y, \Delta z, x_4 - \bar{x}, y_4 - \bar{y}, \phi_1, \theta_1, \psi_1, \phi_2, \theta_2, \psi_2\}^T \tag{50}$$

Since all the dynamic equations are of second order, clearly, each output variable needs to be differentiated twice before one or more of the control variables appear on the right-hand side. To clearly illustrate the procedure for determining the feedback control law, the output is written in the following form:

$$y = [C_1 \quad 0]\begin{Bmatrix} x_1 \\ x_2 \end{Bmatrix} \tag{51}$$

Then the second time derivative of the output is obtained as follows:

$$\dot{y} = C_1 \dot{x}_1 = C_1 E x_2$$

$$\ddot{y} = C_1 \nabla_x (E x_2) \dot{x}$$

$$= C_1 \left[\nabla_{x1}(E x_2) E x_2 + E M^{-1}(\check{r} + S u_{\text{out}})\right] \tag{52}$$

where

$$\check{r}(x_1, x_2, a) = r(x_1, x_2, a) + S(x_1, x_2, a) u_{\text{in}}(x_1, x_2) \tag{53}$$

To decouple and linearize the input-output behavior of the twin-lift system, one would like to have

$$\ddot{y} = v \tag{54}$$

Equating the right-hand sides of Eqs. (52) and (54) gives rise to

$$D u_{\text{out}} = v - f^* \tag{55}$$

where

$$D = C_1 E M^{-1} S, \qquad f^* = C_1 \left[\nabla_{x_1}(E x_2) E x_2 + E M^{-1} \check{r}\right] \tag{56}$$

The expression given by Eq. (55) contains 14 equations in 8 unknowns. This poses a problem in determining a solution for the feedback control, u_{out}. Assuming that rank $(D) = 8$ (i.e., D is full rank), the difficulty is circumvented by using the left inverse of D to solve for u_{out}:

$$u_{\text{out}} = (D^T D)^{-1} D^T (v - f^*) \tag{57}$$

In an event when rank$(D) < 8$, a solution to Eq. (55) can be determined using $D^\dagger$, the generalized (or pseudo) inverse of D. However, in all simulation runs carried out during this study, D was found to be full rank. Equation (57) gives the least-squares approximate solution to Eq. (55). Substituting for the feedback control from Eq. (57) into Eq. (52), it can be observed that the input-output linearization is approximate in the least-squares sense. Tracing the functional dependence of quantities on the right-hand side of Eq. (57), it is found that $u_{\text{out}} = u_{\text{out}}(x_1, x_2, a)$. The value of a required for determining u_{out} is computed from Eq. (41). However, if measurements for the main rotor and tail rotor flapping coefficients are available, then a need not be computed in the actual implementation of the feedback control law.

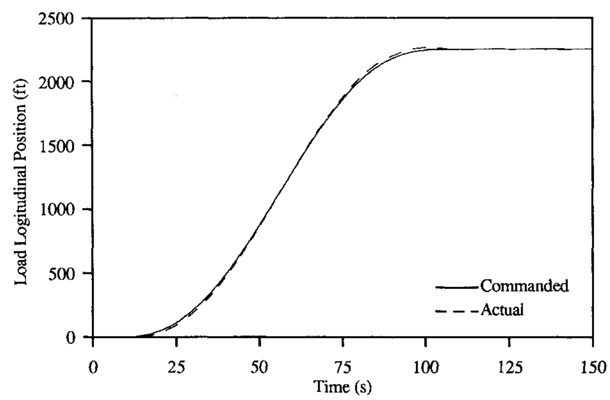

Fig. 5 Load longitudinal position response for a typical twin-lift mission.

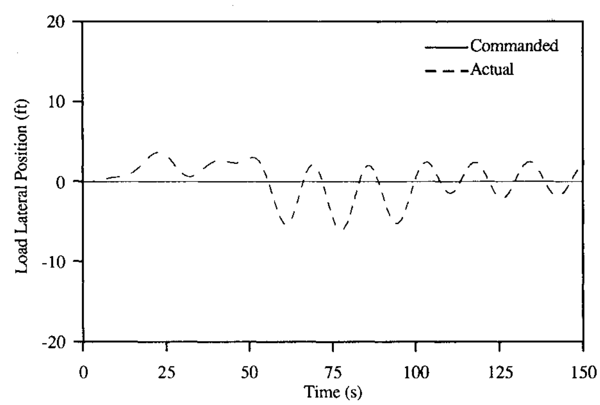

Fig. 6 Load lateral position response for a typical twin-lift mission.

At this stage, additional feedback is imposed on the system to achieve desired output tracking behavior. The feedback gains can be designed using any of the various techniques known from linear control system design. In the present work a combination of proportional, derivative, and integral (PID) feedbacks is imposed for each output loop. This combination provides the designer the capability of adjusting the speed, damping, and tracking accuracy in the response of output variables. Therefore,

$$v = \ddot{y}_c + K_P(y_c - y) + K_D(\dot{y}_c - \dot{y}) + K_I\int_0^t (y_c - y)\,\mathrm{d}t \tag{58}$$

where y_c denotes the commanded value of y. K_P, K_D, and K_I are diagonal matrices consisting of individual loop gains on the diagonals, which can be designed to meet stability and/or performance specifications, if any, for the closed-loop system. A block diagram representation of the twin-lift control structure is provided in Fig. 3.

In this paper the nonlinear controller synthesized previously is validated only for a particular type of twin-lift operation. However, the authors strongly feel that the controller should be able to handle more demanding tasks than those for which results are given in the section on simulation results. Based on the results of two-dimensional analysis,[1,5] it is further noted that the type of controller developed here is capable of tolerating mild uncertainties in the system model. However, for cases in which severe uncertainties are possible in the system model, it is necessary to introduce robustness and/or adaptation capability into the controller in order to obtain satisfactory overall closed-loop performance. One such adaptive control approach has been developed for the two-dimensional case in Ref. 12.

Trim

A considerable effort is needed to determine the trim configuration for the system due to the multitude and complexity of

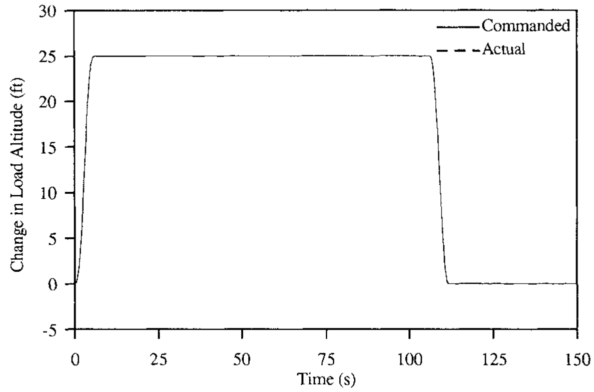

Fig. 7 Load vertical position response for a typical twin-lift mission.

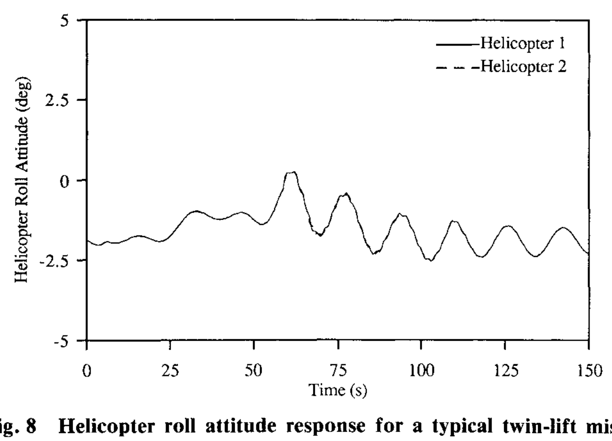

Fig. 8 Helicopter roll attitude response for a typical twin-lift mission.

Table 2 Solution for helicopter trim variables

Variable	Helicopters 1, 2 ($h = 0$), deg	Helicopters 1, 2 ($h = 3.6$ ft), deg	Limits, deg
ϕ	−2.11	−1.9	
θ	5.04	4.3	
θ_0	26.49	26.76	[13, 29]
B_{1s}	1.95	1.22	[−17.7, 17.7]
A_{1s}	−1.76	−2.02	[−11, 11]
$\theta_{0_{TR}}$	29.06	29.53	[−12, 32]

Table 3 PID gains used for nonlinear control

Loop	K_P	K_D	K_I
Δx, $\bar{x}$	0.0625	0.5000	0.0005
Δy, $\bar{y}$	0.2500	0.7100	0.0010
Δz, z_4	1.0000	1.4200	0.1000
$x_4-\bar{x}$, $y_4-\bar{y}$	0.2500	1.0000	0.0000
ϕ_1, ϕ_2	0.0000	5.0000	0.0000
θ_1, θ_2	0.0000	4.0000	0.0000
ψ_1, ψ_2	0.0000	4.5000	0.0000

the equations involved. The nonlinear model is trimmed at the initial condition as follows. The initial condition considered is one of hovering flight characterized by the following at $t = 0$:

$$x_4 = y_4 = z_4 = 0 \text{ ft}$$

$$\psi_1 = \psi_2 = \phi_{c_1} = \theta_{c_1} = \phi_{c_2} = \theta_{c_2} = \phi_3 = \theta_3 = \theta_t = \phi_4 = \theta_4 = 0 \text{ deg}$$

$$\psi_3 = \psi_4 = -45 \text{ deg} \tag{59}$$

where ϕ_{c_i} and θ_{c_i} are, respectively, the roll and pitch attitudes of cable c_i, $i = 1,2$. To complete the definition of the trim configuration, one needs to determine the values of the following variables at $t = 0$: ϕ_1, θ_1, ϕ_2, θ_2, $\theta_0^{(1)}$, $A_{1s}^{(1)}$, $B_{1s}^{(1)}$, $\theta_{0_{TR}}^{(1)}$, $\theta_0^{(2)}$, $A_{1s}^{(2)}$, $B_{1s}^{(2)}$, and $\theta_{0_{TR}}^{(2)}$. The flight condition defined by Eq. (59) closely represents some of the operational configurations of the past. Figure 4 shows the pictorial view of one such configuration used by PLM Helicopters for the Bell Jet Rangers. In this configuration helicopter 1 is ahead and to the right of helicopter 2. It is noted that, for a hypothetical case of $h_1 = h_2 = 0$, the six forces and moments acting at the c.g. of each helicopter are known. The four controls and the pitch and roll attitudes of the helicopter required to generate these forces and moments are then determined by a numerical solution of the six nonlinear algebraic equations comprising the helicopter's aerodynamic model. The trim condition for actual nonzero values of h_1 and h_2 is then determined by using the controller. Closed-loop simulation is run with zero-load motion commands to the controller and with initial conditions the same as those for the case of $h_1 = h_2 = 0$. The simulation is carried out until the accelerations vanish, representing the trim condition.

Results are given for the case employing two UH-60 helicopters. The helicopter aerodynamic model of Ref. 7 is revised to include the UH-60 specific modifications reported in Ref. 13: fuselage aerodynamic force and moment equations that are specific to the UH-60, a canted tail rotor and a horizontal stabilator with variable incidence. The SAS gains in Eq. (44) are derived for the UH-60 helicopter based on the SAS model given in Ref. 14. For the following illustration, all four tethers were assumed to be inelastic. The numerical values of the physical parameters that are used for the analysis are given in Table 1. The trim values of the helicopter attitudes and controls for the hypothetical case of $h_1 = h_2 = 0$, as well as those for the actual case of $h_1 = h_2 = 3.6$ ft, are shown in Table 2. The helicopter control limits are also given in Table 2.

Simulation Results

The twin-lift nonlinear dynamical model as given by Eqs. (47) and (41) is implemented in a numerical simulation. In Eq.

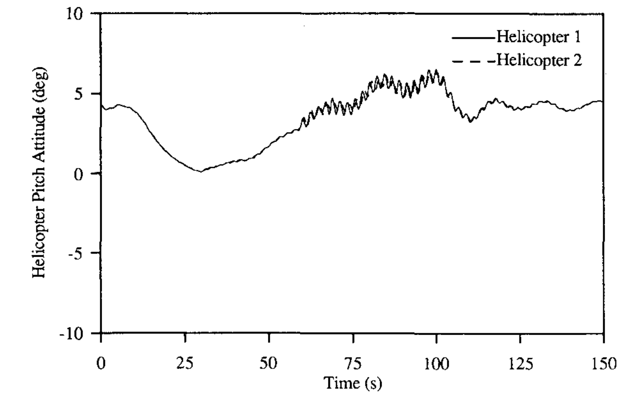

Fig. 9 **Helicopter pitch attitude response for a typical twin-lift mission.**

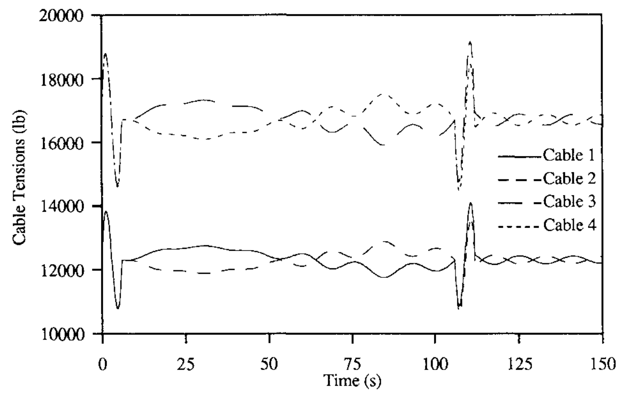

Fig. 11 **Cable tension forces for a typical twin-lift mission.**

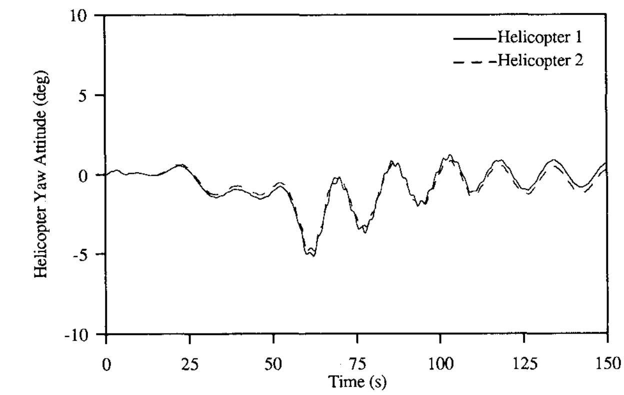

Fig. 10 **Helicopter yaw attitude response for a typical twin-lift mission.**

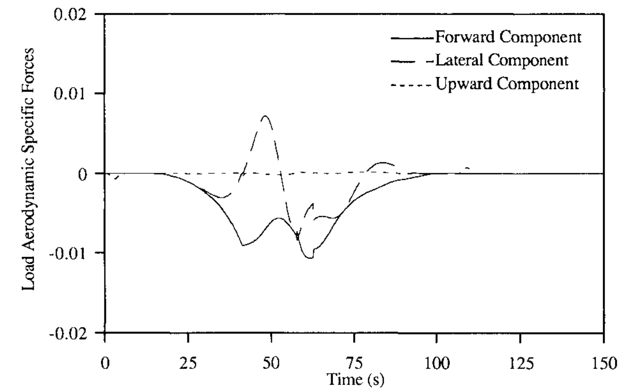

Fig. 12 **Load aerodynamic specific forces for a typical twin-lift mission.**

(47) the velocity dynamics $\dot{x}_2$ are integrated using a modified Euler scheme, whereas the position dynamics $\dot{x}_1$ are integrated using an averaging-type method. These methods are typical of helicopter simulation programs and have been used in the computer program of Ref. 7. A time step of 0.0125 s was found to result in sufficient numerical accuracy in satisfying the kinematic constraints given by Eqs. (12) and (19).

Implementation of the controller requires selection of the PID gains in Eq. (58), which is performed as follows. Ignoring the integral gains, the proportional and derivative gains for the first eight output variables are fixed according to the typical natural frequency and desired damping for these variables. This procedure is not very straightforward since the input-output behavior is not decoupled exactly; a trial-and-error approach is necessary. Then a small integral gain is added for the first six output variables to obtain good steady-state response in the presence of small modeling uncertainties. The derivative gains for the attitude loops are determined by minimal stability requirements during smooth $\bar{x}$, $\bar{y}$, and z_4 commands. The final values of the PID gains used are given in Table 3. The command values for ψ_1 and ψ_2 are chosen to require zero sideslip during any maneuvering, i.e.,

$$\psi_{1_c} = \tan^{-1}\left(\frac{\dot{\bar{y}}_c + 0.5\Delta\dot{y}_c}{\dot{\bar{x}}_c + 0.5\Delta\dot{x}_c}\right), \quad \psi_{2_c} = \tan^{-1}\left(\frac{\dot{\bar{y}}_c - 0.5\Delta\dot{y}_c}{\dot{\bar{x}}_c - 0.5\Delta\dot{x}_c}\right) \tag{60}$$

and the Δx, Δy, and Δz commands are chosen to keep cables c_1 and c_2 vertical, as in the initial condition, i.e.,

$$\Delta x_c = \Delta x^0 = L \sin \pi/4, \quad \Delta y_c = \Delta y^0 = L \cos \pi/4, \quad \Delta z_c = 0 \tag{61}$$

The closed-loop performance is illustrated for a typical twin-lift mission, where the load is required to be lifted vertically up by 25 ft in 6 s, then moved forward by 2250 ft in 100 s, and finally lowered by 25 ft in 6 s. It is felt that this maneuver depicts the more realistic situation of moving a battle tank across a river. The command trajectory for each segment consists of a fifth-order polynomial in time; the coefficients of this polynomial are chosen to obtain zero velocity and acceleration commands at the initial and final times for that segment:

$$\bar{x}_c(t) = \begin{cases} 0 & 0 \le t \le 6 \\ 2250\left[10\left(\dfrac{t-6}{100}\right)^3 - 15\left(\dfrac{t-6}{100}\right)^4 + 6\left(\dfrac{t-6}{100}\right)^5\right] & 6 < t \le 106 \\ 2250 & \text{otherwise} \end{cases}$$

$$\bar{y}_c(t) = 0$$

$$z_{y_c}(t) = \begin{cases} 25\left[10\left(\dfrac{t}{6}\right)^3 - 15\left(\dfrac{t}{6}\right)^4 + 6\left(\dfrac{t}{6}\right)^5\right] & 0 \le t \le 6 \\ 25 & 6 < t \le 106 \\ 25\left[10\left(\dfrac{112-t}{6}\right)^3 - 15\left(\dfrac{112-t}{6}\right)^4 + 6\left(\dfrac{112-t}{6}\right)^5\right] & 106 < t \le 112 \\ 0 & \text{otherwise} \end{cases} \tag{62}$$

Figures 5–12 show closed-loop simulation results of the twin-lift mission. Figure 5 shows that the load tracking in the longitudinal direction is achieved with extremely small undershoot and overshoot at the beginning and the end, respectively, of the segment. The maximum longitudinal speed of ~ 26 kt is attained by the load at the middle of the longitudinal command phase. Figure 6 shows small (as compared to load longitudinal position response) deviations in load lateral position from the zero command value. However, this deviation vanishes in steady state. Note that this deviation is due to the approximate linearization of output dynamics and the inherent coupling in the longitudinal and lateral dynamics of the helicopter. As noticed in Fig. 7, the tracking response for the load vertical position is almost exact. It is found that the regulation of the Δx, Δy, and Δz loops is achieved with tight tolerance, which ensures safety during the mission. Figures 8–10 display the helicopters' roll, pitch, and yaw attitude evolution. The angles remain small during the entire mission. Furthermore, all controls stay within their limits throughout the mission. Figure 11 shows the tension forces in cables c_i, $i = 1, \ldots, 4$. Cables c_1 and c_3 are on the helicopter 1 side of the configuration, and cables c_2 and c_4 are on the side of helicopter 2. During the vertical command phases, the variation in the cable tension forces follows the variation in the collective control very closely. During the longitudinal command phase, the sum of the tension forces in cables c_1 and c_2 and the sum of the tension forces in cables c_3 and c_4, remain approximately constant, close to their respective initial values. This is due to the fact that the principal load supported by the cables is the weight of the payload. The aerodynamic force on the load during the entire mission remains small and negligible compared to the load weight, as seen in Fig. 12. Figure 12 shows that the inertial axis components of the load aerodynamic specific force remain small. The nature of the variation in cable tension forces during the longitudinal command phase can be explained as follows. Notice that during the first half of this phase, the differential cable tension forces $T_1 - T_2$ and $T_3 - T_4$ are positive, whereas the same forces are negative during the second half of the phase. It is observed from the twin-lift geometry that positive values of $T_1 - T_2$ and $T_3 - T_4$ provide forward load acceleration. Thus, the cable tension forces evolve to give rise to forward acceleration to the load during the first half of the command phase and deceleration during the second half. This is in agreement with what is demanded by the load longitudinal position command trajectory, shown in Fig. 5. The quantity $T_1 - T_2$ indicates the relative load sharing by the helicopters during the mission. This difference is bounded by approximately 0.5 ton.

Conclusions

The nonlinear dynamical model of the twin-lift system presented in this paper is very general in nature and includes the possibilities of elastic or inelastic cables. To the authors' knowledge, during the course of this work, the first nonlinear simulation capability for the twin-lift system was developed. For the specific command trajectory considered, simulation results show that the nonlinear controller designed here enables stable load transportation with tight tolerances and reasonable control magnitudes.

References

[1]Prasad, J. V. R., Mittal, M., and Schrage, D. P., "Control of a Twin-Lift Helicopter System Using Nonlinear State Feedback," *Journal of the American Helicopter Society*, Vol. 36, No. 4, Oct. 1991, pp. 57–65.

[2]Cicolani, L. S., and Kanning, G., "Equations of Motion of Slung Load Systems, Including Multi-Lift Systems," NASA TM 1038798, Sept. 1991.

[3]Mittal, M., "Modeling and Control of a Twin-Lift Helicopter System," Ph.D. Dissertation, School of Aerospace Engineering, Georgia Inst. of Technology, Atlanta, GA, Nov. 1991.

[4]Kane, T. R., and Levinson, D. A., *Dynamics: Theory and Applications*, McGraw-Hill, New York, 1985.

[5]Mittal, M., Prasad, J. V. R., and Schrage, D. P., "Comparison of Stability and Control Characteristics of Two Twin-Lift Helicopter Configurations," *Journal of Nonlinear Dynamics*, Vol. 3, No. 3, May 1992, pp. 199–223.

[6]Curtiss, H. C., and Warburton, F. W., "Stability and Control of the Twin Lift Helicopter System," *Journal of the American Helicopter Society*, Vol. 30, No. 2, April 1985, pp. 14–23.

[7]Talbot, P. D., Tinling, B. E., Decker, W. A., and Chen, R. T. N., "A Mathematical Model of a Single Main Rotor Helicopter for Piloted Simulation," NASA TM 84281, Sept. 1982.

[8]Shaughnessy, J. D., Deaux, T. N., and Yenni, K. R., "Development and Validation of a Piloted Simulation of a Helicopter and External Sling Load," NASA TP 1285, Jan. 1979.

[9]McCormick, B. W., *Aerodynamics, Aeronautics, and Flight Mechanics*, Wiley, New York, 1979, p. 196.

[10]Menon, P. K. A., Prasad, J. V. R., and Schrage, D. P., "Nonlinear Control of a Twin-Lift Helicopter Configuration," *Journal of Guidance, Control, and Dynamics*, Vol. 14, No. 6, 1991, pp. 1287–1293.

[11]Asseo, S. J., "Decoupling of a Class of Nonlinear Systems and its Application to an Aircraft Control Problem," *Journal of Aircraft*, Vol. 10, No. 12, 1973, pp. 739–747.

[12]Mittal, M., Prasad, J. V. R., and Schrage, D. P., "Nonlinear Adaptive Control of a Twin Lift Helicopter System," *IEEE Control System Magazine*, Vol. 11, No. 3, April 1991, pp. 39–45.

[13]Hilbert, K. B., "A Mathematical Model of the UH-60 Helicopter," NASA TM 85890, April 1984.

[14]Howlett, J. J., "UH-60A Black Hawk Engineering Simulation Program, Volumes I and II," NASA CR 159084, Nov. 1974.